

Measurement report:

Intra-annual Variability of Black/Brown Carbon and Its Interrelation with Meteorological Conditions over Gangtok, Sikkim

Pramod Kumar¹, Khushboo Sharma¹, Ankita Malu², Rajeev Rajak², Aparna Gupta¹, Bidyutjyoti Baruah¹, Shailesh Yadav¹, Thupstan Angchuk¹, Jayant Sharma¹, Rakesh Kumar Ranjan^{1#}, Anil Kumar Misra¹, and Nishchal Wanjari¹

¹DST's Centre of excellence on Water Resources, Cryosphere and Climate Change Studies, Department of Geology, Sikkim University, Gangtok, Sikkim, India -737102

²Department of Geology, Sikkim University, Gangtok, Sikkim, India -737102

#Corresponding Author: rkranjan@cus.ac.in

S1 Methodology

S1.1 Black carbon and Brown carbon Analysis

The Aethalometer AE33 is an optical instrument that provides real-time measurements of aerosol light absorption and reports black carbon (BC) concentrations (Dutt et al., 2018; Gupta et al., 2017). Specifically, the AE33 can measure BC concentrations in atmospheric particulate matter (PM) with a diameter of 2.5 micrometres (PM_{2.5}) (Dutt et al., 2018).

To collect aerosol particles, the Aethalometer model AE33 draws a stream of aerosol-filled air through a spot on a filter tape. It then analyzes the transmission of light through the sample-containing filter tape and compares it to the transmission of light through an unloaded part of the filter tape, which serves as a reference zone for detecting the aerosol (Sharma et al., 2022). The instrument measures the amount of light that passes through the sample-filled filter, and calculates the attenuation coefficient (ATN) by analyzing how quickly the attenuation changes over time. The attenuation of light, which is proportional to the BC mass concentration, can be calculated using Equation 3.1.

$$ATN = -100 \times \ln \frac{I}{I_0} \quad \text{Eq. (3.1)}$$

The attenuation coefficient (ATN) is defined as the ratio of the intensity of light transmitted through a loaded filter (I) to the intensity of light transmitted through an unloaded reference portion (I₀).

$$b_{ATN} = \frac{A}{Q} \times \left(\frac{1}{100} \right) \times \left(\frac{\Delta ATN}{\Delta t} \right) \quad \text{Eq. (3.2)}$$

Where, A is the spot size, Q is the flow into the instrument, Δt is the change in time (Karakoti et al., 2022).

The scattering of light can impact the optical absorption of aerosols on the filter, and this is quantified by the factor C, which is dependent on the filter material (Weingartner et al., 2003). It's worth noting that the aerosol absorption coefficient (b_{abs}) can be significantly different from the actual concentration of airborne particles. To account for this, calibration factors C (with a multiple scattering parameter of 1.57) and R (ATN) are added to translate aethalometer attenuation readings to actual absorption coefficients (Gupta et al., 2022; Gupta et al., 2017; Aruna et al., 2014; Weingartner et al., 2003).

$$b_{abs} = b_{ATN} / C \cdot R (ATN) \quad \text{Eq. (3.3)}$$

Two variables, C and R, can modify the optical properties of the filter. Due to the multiple scatterings of light, the value of C is typically greater than one. Therefore, the aethalometer output data can be expressed using equation (3.4), which involves converting the attenuation coefficient to the absorption coefficient, and then calculating the mass-equivalent black carbon

concentration by dividing the absorption coefficient by the BC-specific mass absorption cross-section (Petzold et al., 1997). ATN and BC relationship is given in figure (S7) for the daily data.

$$B(\lambda) = \frac{b_{abs} \lambda}{\sigma_{abs} \lambda} \quad \text{Eq. (3.4)}$$

The absorption coefficient ($b_{abs}(\lambda)$) is measured in meters to the power of negative one (m^{-1}), and the mass absorption cross-section in air ($\sigma_{abs}(\lambda)$) is expressed in meters squared per gram ($m^2 g^{-1}$). For the AE-33 model, the value of σ at a wavelength of 880 nm is constant and set at $7.77 m^2 g^{-1}$ (Petzold et al. 1997, Weingartner et al. 2003, Martinsson et al., 2017).

Sandradewi et al. (2008) presents a comprehensive overview of the aethalometer, while Drinovec et al. (2015) discusses its applications (Sharma et al., 2022). The Aethalometer AE33 measures the absorption of light by aerosol particles at seven wavelengths that range from near-infrared to near-ultraviolet (370, 470, 525, 590, 660, 880, and 950 nm). The 880nm signal is used to calculate the total BC mass (Dutt et al., 2018; Gupta et al., 2017). Real-time BC concentrations are calculated using the rate of change of light absorption with a 2-minute temporal resolution (Dutt et al., 2018; Drinovec et al., 2015). Channel 6 data (measured at 880 nm) is utilized as a reference standard to report black carbon concentrations, as the absorption at this wavelength is mainly attributed to BC alone, with other aerosols absorbing relatively little at 880 nm (Drinovec et al., 2015; Sandradewi et al., 2008a). Additionally, using the Sandradewi et al. (2008) model, the equipment also contributes traces of biomass burning/fossil fuel combustion to black carbon concentration in ambient air due to variations in the spectrum dependencies of the absorption coefficients, as given in equation 3.5.

$$b_{abs}(\lambda) = b_{absff}(\lambda) + b_{absbb}(\lambda) \quad \text{Eq. (3.5)}$$

Based on Sandradewi et al. (2008a), it is assumed that the overall absorption of aerosol light comes from biomass burning or fossil fuel combustion as reported by Martinsson et al. (2017).

S1.2 Source apportionment

BC measurements at 470 nm and 950 nm wavelengths can serve as indicators of local fossil fuel combustion and biomass burning, and therefore help identify their possible sources (Gupta et al., 2022; Kumar et al., 2018; Gupta et al., 2017; Kirchstetter et al. 2004). By measuring the absorption frequency across the 370-950 nm range, it is possible to estimate the contribution of these sources to the total aerosol absorption. The values of σ_{abs} can then be used to derive

the absorption wavelength exponents (α_{abs}) at seven different wavelengths (Moosmüller et al., 2011b; Ganguly et al., 2005; Krichester et al., 2004).

$$\beta_{abs}(\lambda) = K \cdot \lambda^{-\alpha} \quad \text{Eq. (3.6)}$$

where β_{abs} denote mass absorption efficiency, K denotes a constant, λ is the light wavelength, and α is the absorption Angstrom exponent (AAE).

The percentage fractionation of BC was calculated using the Sandradewi et al., 2008 model. The aerosol optical absorption coefficient has specific values of the absorption angstrom exponent, which sums the contributions to aerosol absorption from burning biomass and burning fossil fuels (AAE). The two sources (biomass burning and fossil fuel) have spectral dependence of λ^{-1} and λ^{-2} , respectively (Favez et al., 2010; Sandradewi et al., 2008, Kirchstetter et al., 2004). For source apportionment, the wavelengths 470 and 950 nm were chosen (Sandradewi et al., 2008), where λ_1 is 470 and λ_2 is 950. The absorption dependence of various particles was used to compute the contributions of $\beta_{abs_{bb}}$ (biomass) and $\beta_{abs_{ff}}$ (fossil fuel) at two distinct wavelengths (λ_1, λ_2) (Gupta et al., 2022).

The Sandradewi et al. (2008) model was used to calculate the fractionation percentage of BC. The model includes specific values of the absorption angstrom exponent (AAE), which accounts for the contributions to aerosol absorption from burning biomass and burning fossil fuels. Biomass burning and fossil fuel sources have spectral dependencies of λ^{-1} and λ^{-2} , respectively (Kirchstetter et al., 2004; Favez et al., 2010; Sandradewi et al., 2008). The wavelengths of 470 nm and 950 nm were chosen for source apportionment, where λ_1 is 470 and λ_2 is 950 (Sandradewi et al., 2008). The contributions of $\beta_{abs_{bb}}$ (biomass) and $\beta_{abs_{ff}}$ (fossil fuel) at these two wavelengths (λ_1 and λ_2) were calculated using the absorption dependence of various particles (Gupta et al., 2022).

$$\frac{b_{abs}(\lambda_1)_{ff}}{b_{abs}(\lambda_2)_{ff}} = \left(\frac{\lambda_1}{\lambda_2}\right) - aff \quad \text{Eq. (3.7)}$$

$$\frac{b_{abs}(\lambda_1)_{bb}}{b_{abs}(\lambda_2)_{bb}} = \left(\frac{\lambda_1}{\lambda_2}\right) - abb \quad \text{Eq. (3.8)}$$

The fractionation of β_{bb} (biomass burning) at 950 nm and β_{ff} (fossil fuel combustion) at 470 nm was estimated using the following equation.

$$b_{abs}(\lambda) = b_{abs}(\lambda)_{ff} + b_{abs}(\lambda)_{bb} \quad \text{Eq. (3.9)}$$

Where, β_{bb} represents the spectrally dependent mass absorption efficiency and β_{ff} represents the spectrally dependent mass absorption efficiency at 880 nm.

$$BB(\%) = \frac{b_{abs}(\lambda_2)_{bb}}{b_{abs}(\lambda_2)} \quad \text{Eq. (3.10)}$$

$$BC_{bb} = BB \times BC \quad \text{Eq. (3.11)}$$

$$B_{ff} = (1 - BB) \times BC \quad \text{Eq. (3.12)}$$

The average concentration of light-absorbing carbon particles was determined by taking readings from the aethalometer at different wavelengths. Various studies have reported BC_{ff} values around 1 and BC_{bb} values approximately 2 (Kant et al., 2020; Zotter et al., 2017; Herich et al., 2011; Sandradewi et al., 2008b).

S1.3 LULC calculation

The LULC calculation using Landsat data methodology is performed using QGIS. Here is a summary of the methodology used for the LULC. (1) Imported Landsat data, (2) Pre-processing of Landsat data to remove any noise or distortions using Semi-Automatic Classification Plugin (SCP). This typically involves atmospheric correction, radiometric calibration, and geometric correction. (3) Image classification tools used to assign each pixel in the Landsat image to a specific land cover or land use class. This is done using various classification algorithms, such as maximum likelihood, support vector machine (SVM), and random forest. (4) Ground truthing has used collected field data to validate the accuracy, and google map used for cross check. (5) Post-processing was utilized to refine the image classification results to remove any errors or inconsistencies using the Geographic Resources Analysis Support System (GRASS). This is completed using method, spatial smoothing, and object-based analysis. (6) LULC mapping for creating a map of the land cover and land use classes in the present study area based on the image classification results using the Semi-Automatic Classification Plugin (SCP).

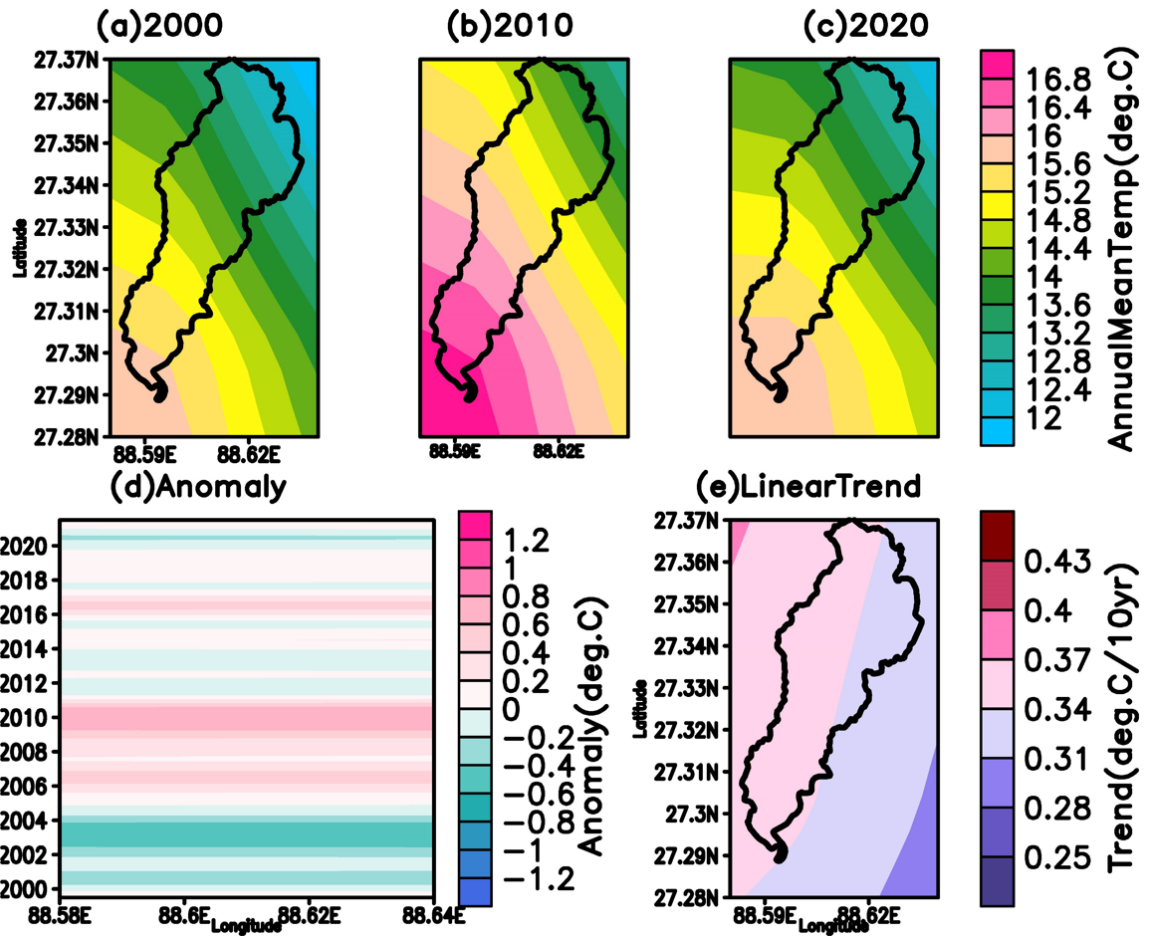


Figure S1. Spatiotemporal variation of temperature (2meter) for 2000 to 2020. Figures (a, b, and c) are annual average temperature for the year 2000, 2010, and 2020 respectively. Figure (d) is anomaly over Gangtok region, and (e) the decadal trend of temperature for 2000 to 2021 over entire Gangtok region.

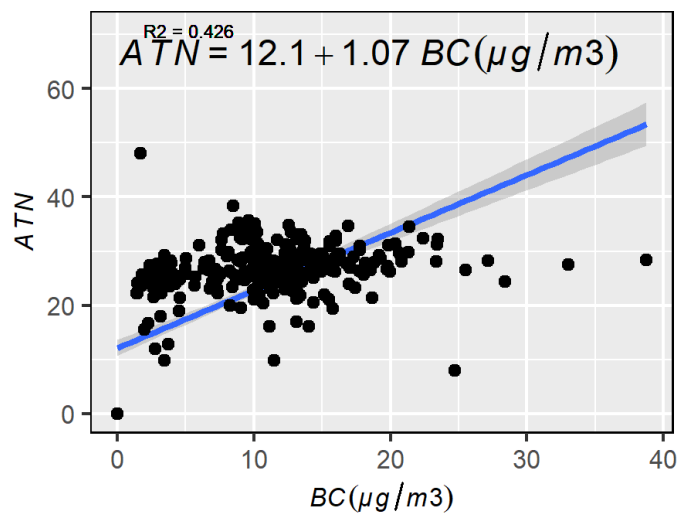


Figure S2. The relationship between and attenuation (ATN) vs black carbon (BC) for daily.

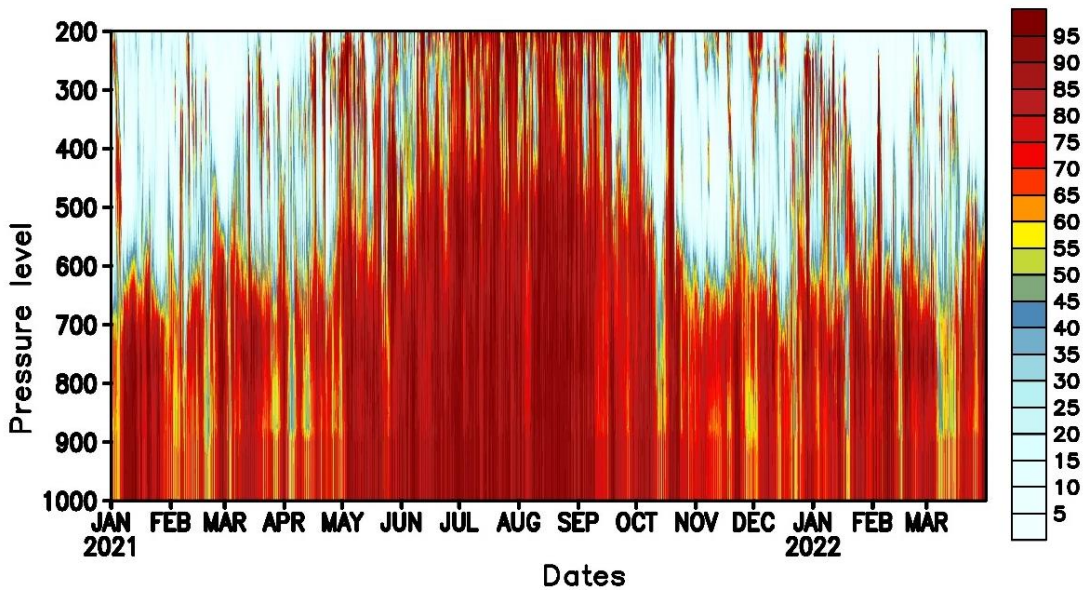


Figure S3. The daily relative humidity on pressure level for 1st January 2021 to 31st March 2022 over study location (lat:27.32; lon:88.61).

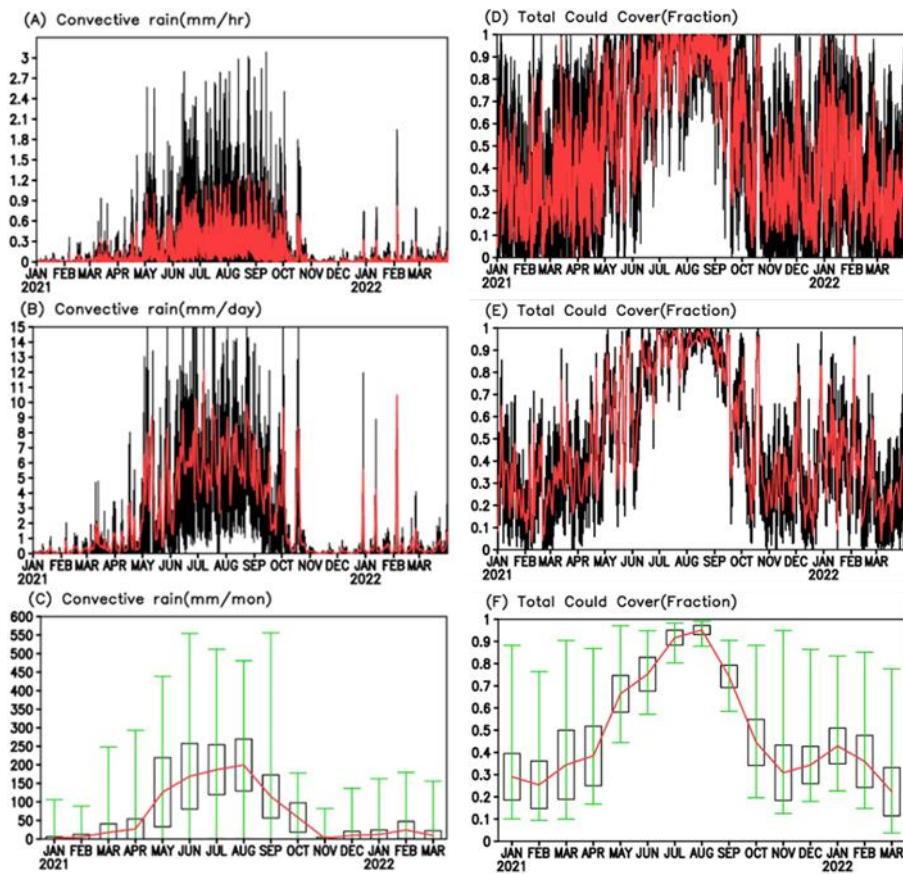


Figure S4. The convective rain for (A) hourly, (B) daily, (C) monthly and total cloud cover (D) hourly, (E) daily, (F) monthly for 1st January 2021 to 31st March 2022 over study location (lat:27.32; lon:88.61).

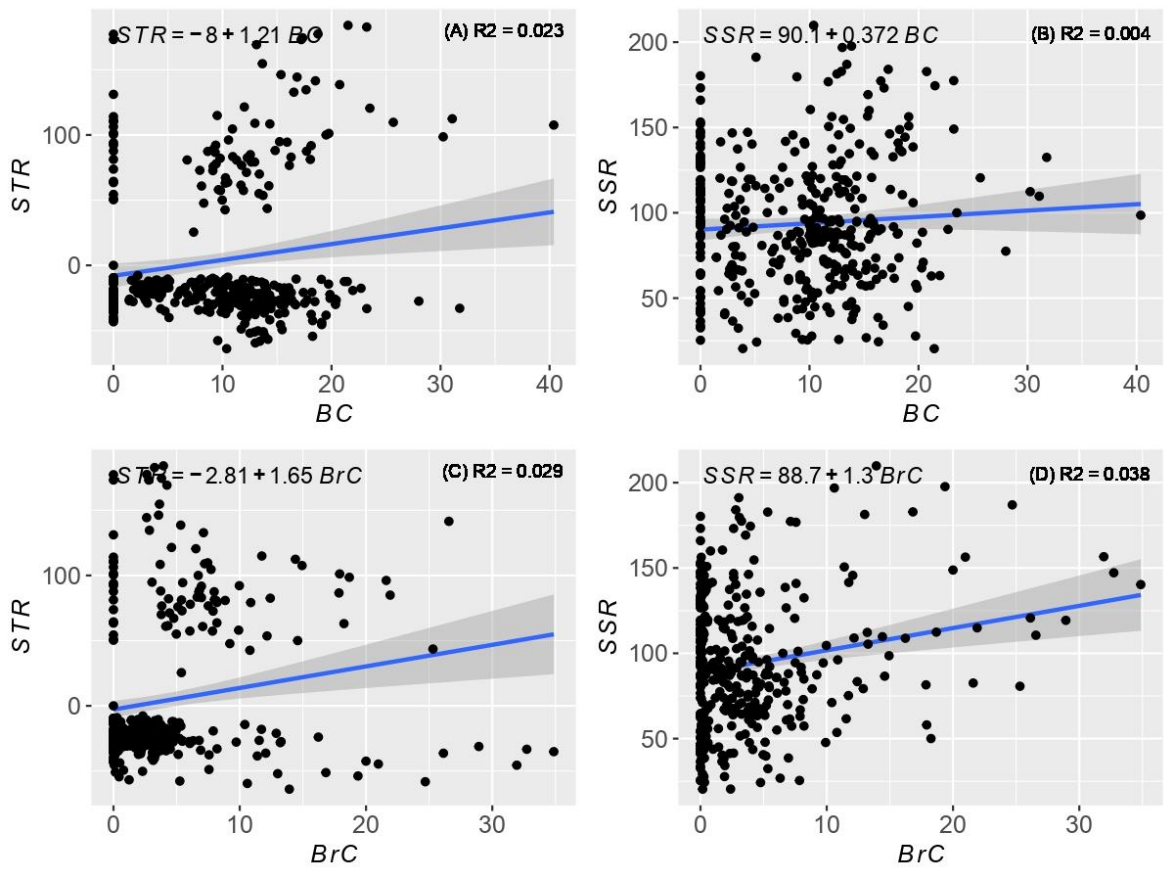


Figure S5. Inter-relationship in net solar and thermal radiation downward (SSR and STR) to Black Carbon and Brown Carbon (BC and BrC); (A) for BC and STR, (B) for BC and SSR, (C) for BrC and STR, and (D) BrC and SSR.

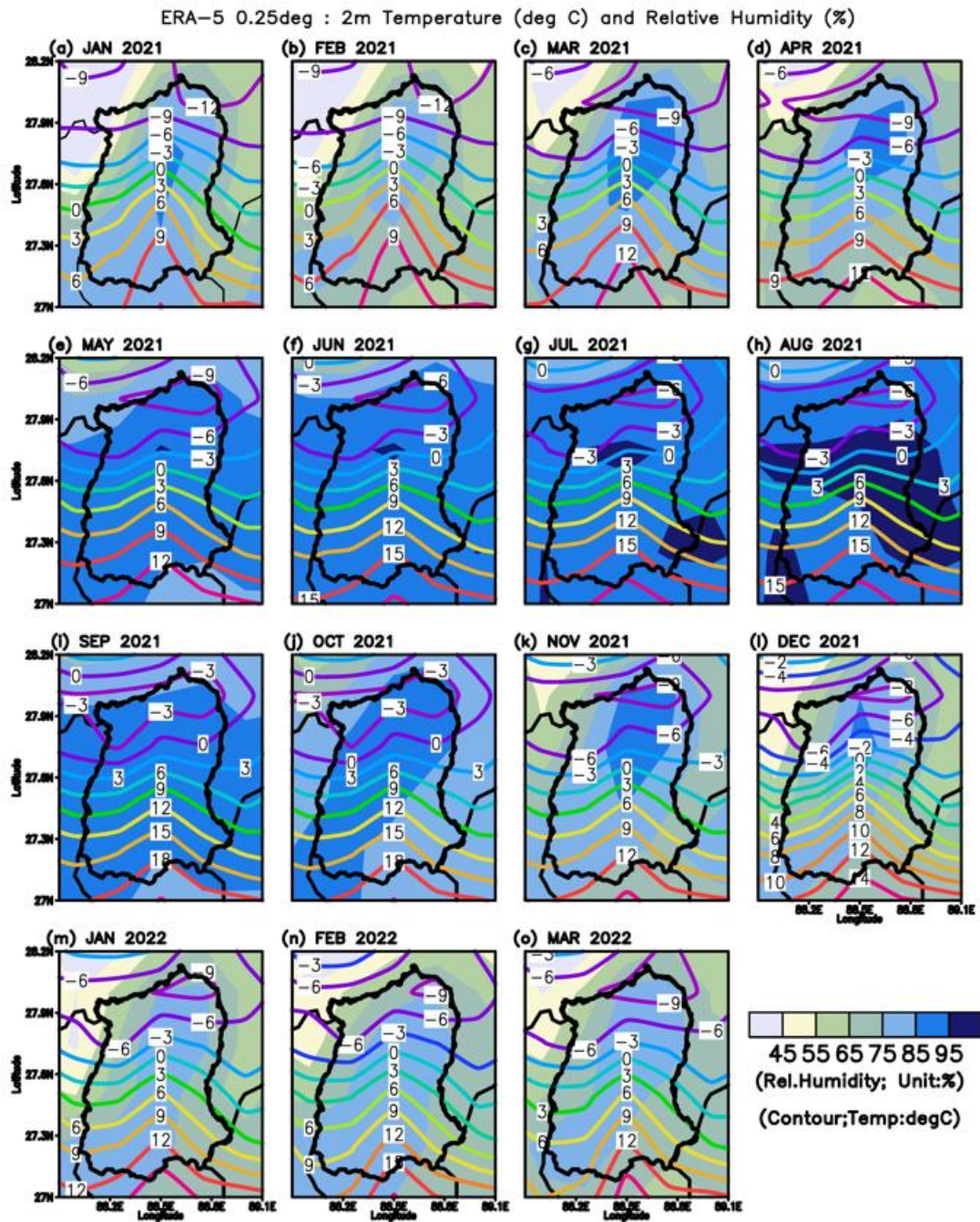


Figure S6. Monthly relative humidity and 2m mean temperature pattern during January 2021 to March 2022. The shading shows precipitation pattern, and streamline shows wind circulation.

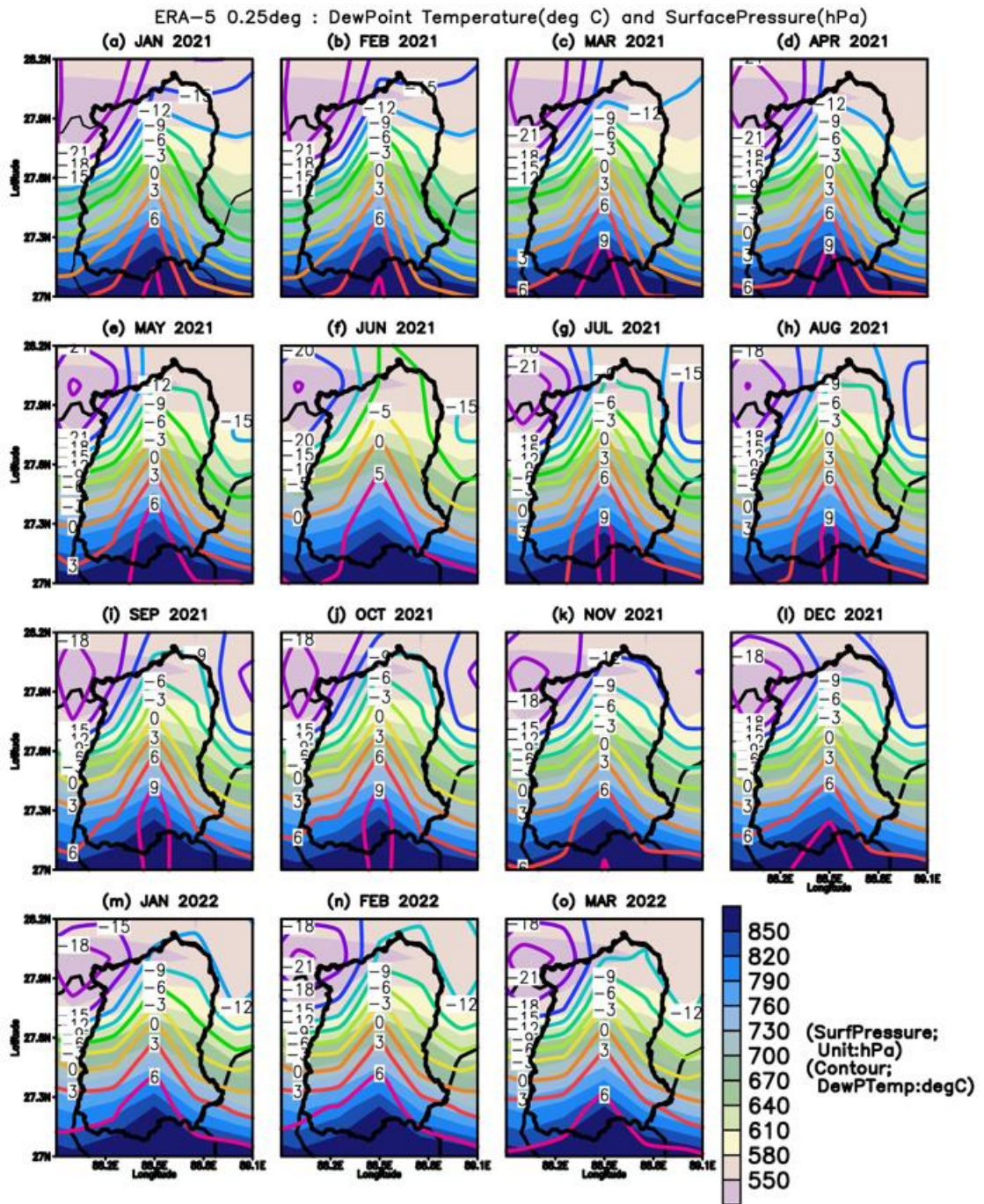


Figure S7. Monthly surface pressure and dewpoint temperature pattern during January 2021 to March 2022. The shading shows precipitation pattern, and streamline shows wind circulation.

Table S1. The population change for three decades over the Sikkim.

Year	2001	2011	2019	References (footnote)
Population	5,40,851	6,10,577	6,90,251	Indian Census (https://censusindia.gov.in/census.website/data/census-tables); (https://statisticstimes.com/demographics/india/sikkim-population.php)
Growth (absolute)	69,726		79,674	Indian Census (https://censusindia.gov.in/census.website/data/census-tables); (https://statisticstimes.com/demographics/india/sikkim-population.php)
Rate (%)	12.9		13.05	https://statisticstimes.com/demographics/india/sikkim-population.php

Table S2. The diurnal data sets of the BC, BCbb, BCff, BrC, BB% CO₂.

Time	BC	BCbb	BCff	BrC	BB%	CO ₂
1	8.81	0.34	7.99	1.18	5.53	344.02
2	6.14	0.33	5.56	1.47	7.16	342.19
3	5.16	0.36	4.54	1.47	9.45	341.24
4	4.78	0.38	4.01	1.49	10.41	340.76
5	5.79	0.32	5.20	0.89	6.64	341.28
6	7.38	0.33	6.90	0.71	5.49	343.07
7	10.75	0.36	10.25	0.24	4.04	346.40
8	16.91	0.38	16.34	0.00	2.76	349.87
9	20.18	0.46	19.57	0.00	2.83	352.68
10	15.99	0.69	15.05	2.95	4.78	354.45
11	12.09	0.80	11.07	4.08	8.40	351.10
12	8.52	0.69	7.62	3.77	10.26	343.69
13	5.44	0.56	4.72	2.82	12.88	336.78
14	4.44	0.46	3.80	2.24	13.31	334.01
15	3.91	0.45	3.34	2.12	14.12	331.98
16	3.82	0.44	3.33	2.18	14.80	330.86
17	4.30	0.46	3.60	2.30	14.44	332.14
18	6.19	0.53	5.46	2.57	12.44	334.34
19	10.47	0.73	9.57	3.17	9.85	342.46
20	14.67	0.82	13.52	3.93	8.44	346.65
21	17.23	0.83	15.81	3.29	7.72	349.23
22	19.76	0.66	17.85	1.79	5.17	349.87
23	18.27	0.48	17.16	1.49	4.84	349.04
24	12.98	0.37	11.74	1.64	5.08	346.01

Table S3. The monthly data set and basic statistics.

Months	Variables	Minimum	Mean	Maximum	Standard Error	Standard Deviation
Mar-21	BC	10.03	12.59	18.14	0.50	1.99
	BCbb	0.90	2.39	4.90	0.28	1.11
	BCff	7.81	10.19	16.63	0.50	2.00
	BrC	2.21	14.10	31.94	2.07	8.27
	BB%	7.49	19.89	33.20	2.00	8.02
	CO2	347.35	356.20	379.35	2.42	10.53
Apr	BC	4.33	12.98	31.76	2.14	7.42
	BCbb	1.16	2.51	3.63	0.22	0.77
	BCff	1.47	10.47	28.91	2.09	7.25
	BrC	5.46	17.46	34.87	2.87	9.93
	BB%	10.69	22.86	44.44	2.70	9.34
	CO2	346.95	355.43	370.37	1.21	6.54
May	BC	3.47	6.28	14.59	0.48	2.53
	BCbb	0.34	0.62	0.88	0.03	0.17
	BCff	2.66	5.66	13.86	0.49	2.57
	BrC	1.43	3.03	5.34	0.23	1.20
	BB%	5.43	13.02	24.28	0.99	5.26
	CO2	344.21	350.98	356.02	0.83	3.98
Jun	BC	1.45	2.86	3.88	0.12	0.66
	BCbb	0.19	0.47	0.90	0.03	0.17
	BCff	1.16	2.40	3.39	0.10	0.56
	BrC	0.94	2.91	11.72	0.36	1.95
	BB%	10.10	16.52	24.86	0.72	3.85
	CO2	336.43	345.14	352.40	0.76	4.09
Jul	BC	1.47	9.12	15.92	0.98	4.72
	BCbb	0.00	0.21	0.89	0.04	0.19
	BCff	1.31	8.91	15.74	1.01	4.82
	BrC	0.00	0.98	7.90	0.38	1.85
	BB%	0.00	4.85	20.08	1.30	6.22
	CO2	338.62	344.93	353.09	0.63	3.35
Aug	BC	7.65	10.28	15.17	0.42	1.97
	BCbb	0.01	0.15	0.28	0.01	0.07
	BCff	7.43	10.12	15.06	0.42	1.99
	BrC	0.00	0.34	1.00	0.06	0.30
	BB%	0.15	2.18	4.03	0.21	0.99
	CO2	335.69	342.22	350.52	0.64	3.57
Sep	BC	7.81	12.30	22.70	0.62	3.41
	BCbb	0.04	0.15	0.44	0.02	0.10
	BCff	7.61	12.15	22.62	0.62	3.42
	BrC	0.00	0.47	4.72	0.16	0.89
	BB%	0.66	2.22	7.75	0.25	1.39
	CO2	335.53	344.79	359.53	0.88	4.76
Oct	BC	3.11	16.58	28.01	1.01	5.24
	BCbb	0.00	0.24	0.63	0.03	0.16

	BCff	3.11	16.34	27.59	1.01	5.25
	BrC	0.00	0.67	3.25	0.14	0.75
	BB%	0.00	2.81	11.50	0.48	2.50
	CO2	340.00	350.36	362.40	0.94	5.22
Nov	BC	5.64	12.09	18.20	0.58	3.18
	BCbb	0.20	0.67	1.42	0.06	0.32
	BCff	5.07	11.42	17.70	0.59	3.24
	BrC	0.59	3.02	6.91	0.31	1.68
	BB%	4.54	8.89	13.55	0.50	2.71
	CO2	335.52	341.30	346.61	0.57	3.14
Dec	BC	6.76	13.53	20.37	0.58	3.22
	BCbb	0.24	0.89	2.65	0.08	0.47
	BCff	5.64	12.64	19.89	0.61	3.40
	BrC	1.24	5.53	21.60	0.74	4.13
	BB%	4.11	10.47	24.96	0.81	4.51
	CO2	335.00	339.62	344.69	0.45	2.49
Jan-22	BC	7.36	11.38	19.75	0.49	2.75
	BCbb	0.57	1.33	3.61	0.11	0.63
	BCff	6.54	10.06	17.15	0.48	2.67
	BrC	3.83	8.87	25.30	0.91	5.07
	BB%	6.47	14.20	24.97	0.77	4.27
	CO2	329.87	336.73	340.41	0.43	2.42
Feb-22	BC	9.16	14.32	18.52	0.87	3.25
	BCbb	0.67	1.32	2.74	0.15	0.57
	BCff	7.96	13.00	16.72	0.86	3.23
	BrC	3.05	8.56	26.56	1.90	7.10
	BB%	7.00	11.36	19.93	1.08	4.03
	CO2	332.81	336.74	343.82	0.67	2.92
Mar-22	BC	13.12	21.52	40.39	1.72	7.08
	BCbb	0.80	1.57	3.65	0.22	0.93
	BCff	12.23	19.95	36.74	1.51	6.24
	BrC	2.63	6.32	18.68	1.19	4.92
	BB%	6.97	10.03	17.97	0.69	2.85
	CO2	NA	NA	NA	NA	NA

Data link for the data access:

https://docs.google.com/spreadsheets/d/1N4F_ft68syY6n0UIfA6nzI5o-8LUWjyFfk5NpfquRyg/edit?usp=sharing

References

- Aruna, K., Kumar, T. L., Rao, D. N., Murthy, B. K., Babu, S. S., & Krishnamoorthy, K. (2014). Scattering and absorption characteristics of atmospheric aerosols over a semi-urban coastal environment. *Journal of Atmospheric and Solar-Terrestrial Physics*, 119, 211-222. <https://doi.org/10.1016/j.jastp.2014.08.009>
- Favez, O., El Haddad, I., Piot, C., Boréave, A., Abidi, E., Marchand, N., ... & D'anna, B. (2010). Inter-comparison of source apportionment models for the estimation of wood burning aerosols during wintertime in an Alpine city (Grenoble, France). *Atmospheric Chemistry and Physics*, 10(12), 5295-5314. <https://doi.org/10.5194/acp-10-5295-2010>
- Ganguly, D., Gadhavi, H., Jayaraman, A., Rajesh, T. A., & Misra, A. (2005). Single scattering albedo of aerosols over the central India: Implications for the regional aerosol radiative forcing. *Geophysical research letters*, 32(18). <https://doi.org/10.1029/2005GL023903>
- Herich, H., Hueglin, C., & Buchmann, B. (2011). A 2.5 year's source apportionment study of black carbon from wood burning and fossil fuel combustion at urban and rural sites in Switzerland. *Atmospheric Measurement Techniques*, 4(7), 1409. [doi:10.5194/amt-4-1409-2011](https://doi.org/10.5194/amt-4-1409-2011)
- Kant, Y., Shaik, D. S., Mitra, D., Chandola, H. C., Babu, S. S., & Chauhan, P. (2020). Black carbon aerosol quantification over north-west Himalayas: Seasonal heterogeneity, source apportionment and radiative forcing. *Environmental Pollution*, 257, 113446. <https://doi.org/10.1016/j.envpol.2019.113446>
- Karakoti, I., Singh, N., Shukla, T., Gairola, A. C., & Dobhal, D. P. (2022). Characterization and source apportionment of black carbon over a valley glacier at transitional climatic zone of the central-western Himalaya. *Theoretical and Applied Climatology*, 1-15. <https://doi.org/10.1007/s00704-022-04313-z>
- Martinsson, J., Abdul Azeem, H., Sporre, M.K., Bergström, R., Ahlberg, E., Öström, E., Kristensson, A., Swietlicki, E. and Eriksson Stenström, K. (2017). Carbonaceous aerosol source apportionment using the Aethalometer model—evaluation by radiocarbon and levoglucosan analysis at a rural background site in southern Sweden. *Atmospheric Chemistry and Physics*, 17(6), 4265-4281. <https://doi.org/10.5194/acp-17-4265-2017>
- Moosmüller, H., & Chakrabarty, R. K. (2011b). Simple analytical relationships between Ångström coefficients of aerosol extinction, scattering, absorption, and single scattering albedo. *Atmospheric Chemistry and Physics*, 11(20), 10677-10680. <https://doi.org/10.5194/acp-11-10677-2011>
- Petzold, A., Kopp, C., & Niessner, R. (1997). The dependence of the specific attenuation cross-section on black carbon mass fraction and particle size. *Atmospheric Environment*, 31(5), 661-672. [https://doi.org/10.1016/S1352-2310\(96\)00245-2](https://doi.org/10.1016/S1352-2310(96)00245-2)
- Weingartner, E., Saathoff, H., Schnaiter, M., Streit, N., Bitnar, B., & Baltensperger, U. (2003). Absorption of light by soot particles: determination of the absorption coefficient by means of aethalometers. *Journal of Aerosol Science*, 34(10), 1445-1463. [https://doi.org/10.1016/S0021-8502\(03\)00359-8](https://doi.org/10.1016/S0021-8502(03)00359-8)
- Zotter, P., Herich, H., Gysel, M., El-Haddad, I., Zhang, Y., Močnik, G., ... & Prévôt, A. S. (2017). Evaluation of the absorption Ångström exponents for traffic and wood burning in the

Aethalometer-based source apportionment using radiocarbon measurements of ambient aerosol. *Atmospheric Chemistry and Physics*, 17(6), 4229-4249. <https://doi.org/10.5194/acp-17-4229-2017>